(4)

TECHNICAL REPORT NO. 13

TO

The Office of Naval Research
Contract No. N00014-86-K-0381

POROSITY AND CRACK INITIATION DURING LOW CYCLE FATIGUE

D. A. Gerard+ and D. A. Koss

Department of Materials Science and Engineering
The Pennsylvania State University
University Park, PA 16802

+Currently: General Motors Technical Center,
Warren, MI 48090

SECURITY CLASSIFICATION OF THIS PAGE

REPORT DOCUMENTATION PAGE

1a. REPORT SECURITY CLASSIFICATION UNCLASSIFIED	1b. RESTRICTIVE MARKINGS
2a. SECURITY CLASSIFICATION AUTHORITY	3. DISTRIBUTION/AVAILABILITY OF REPORT Distribution of this document is unlimited.
2b. DECLASSIFICATION/DOWNGRADING SCHEDULE	
4. PERFORMING ORGANIZATION REPORT NUMBER(S) Report No. 13	5. MONITORING ORGANIZATION REPORT NUMBER(S)
6a. NAME OF PERFORMING ORGANIZATION The Pennsylvania State Univ.	6b. OFFICE SYMBOL (If applicable)
6c. ADDRESS (City, State and ZIP Code) Dept. of Materials Science & Engineering The Pennsylvania State University University Park, PA 16802	7a. NAME OF MONITORING ORGANIZATION 7b. ADDRESS (City, State and ZIP Code)
8a. NAME OF FUNDING/SPONSORING ORGANIZATION Office of Naval Research	8b. OFFICE SYMBOL (If applicable)
8c. ADDRESS (City, State and ZIP Code) Office of Naval Research, Code 1131 800 N. Quincy Street Arlington, VA 22217	9. PROCUREMENT INSTRUMENT IDENTIFICATION NUMBER N00014-86-K-0381
	10. SOURCE OF FUNDING NOS. PROGRAM ELEMENT NO. / PROJECT NO. / TASK NO. / WORK UNIT NO.
11. TITLE (Include Security Classification) Porosity and Crack Initiation During Low Cycle Fatigue	
12. PERSONAL AUTHOR(S) D. A. Gerard and D. A. Koss	
13a. TYPE OF REPORT	13b. TIME COVERED FROM _____ TO _____
14. DATE OF REPORT (Yr., Mo., Day) July 1989	15. PAGE COUNT 22
16. SUPPLEMENTARY NOTATION	

17. COSATI CODES		
FIELD	GROUP	SUB. GR

18. SUBJECT TERMS (Continue on reverse if necessary and identify by block number)
Porosity
Fatigue crack initiation
Low cycle fatigue
Powder processed titanium
Void defects

19. ABSTRACT (Continue on reverse if necessary and identify by block number)

The influence of porosity on crack initiation during low cycle fatigue LCF has been examined by both experimental observations and theoretical modeling. Experimental data based on powder-processed titanium indicate a porosity-induced enhancement of crack initiation, which contributes to significant reductions in low cycle fatigue life. All of the levels of porosity examined, which range from 0.4 to 6 volume percent, cause an order of magnitude or greater decrease in the number of cycles to initiate a 15 micron crack.

Based on a modification of a Neuber analysis, local strain profiles which develop adjacent to holes in uniaxial tension and large-strain amplitude fatigue testing have also been predicted and experimentally verified. Modeling porosity located at a surface as a through-thickness hole deforming under plane-stress conditions, adapting a Coffin-Manson law as a failure criterion and using cumulative damage theory, a theoretical analysis has been developed for predicting the number of cycles for microcrack initiation in the presence of porosity. The predictions, which rely on pore shapes and the low cycle fatigue response of the fully dense matrix, accurately predict the number of cycles necessary to initiate a 15 micron crack adjacent to both isolated and interconnected pores during low cycle fatigue.

20. DISTRIBUTION/AVAILABILITY OF ABSTRACT UNCLASSIFIED/UNLIMITED [X] SAME AS RPT [ ] DTIC USERS [ ]	21. ABSTRACT SECURITY CLASSIFICATION UNCLASSIFIED
22a. NAME OF RESPONSIBLE INDIVIDUAL Donald A. Koss	22b. TELEPHONE NUMBER (Include Area Code) 814-865-5447 / 22c. OFFICE SYMBOL

DD FORM 1473, 83 APR EDITION OF 1 JAN 73 IS OBSOLETE.

SECURITY CLASSIFICATION OF THIS PAGE

POROSITY AND CRACK INITIATION DURING LOW CYCLE FATIGUE

D. A. Gerard[+] and D. A. Koss
Department of Materials Science and Engineering
The Pennsylvania State University
University Park, PA 16802

ABSTRACT

The influence of porosity on crack initiation during low cycle fatigue LCF has been examined by both experimental observations and theoretical modeling. Experimental data based on powder-processed titanium indicate a porosity-induced enhancement of crack initiation, which contributes to significant reductions in low cycle fatigue life. All of the levels of porosity examined, which range from 0.4 to 6 volume percent, cause an order of magnitude or greater decrease in the number of cycles to initiate a 15 micron crack.

Based on a modification of a Neuber analysis, local strain profiles which develop adjacent to holes in uniaxial tension and large-strain amplitude fatigue testing have also been predicted and experimentally verified. Modeling porosity located at a surface as a through-thickness hole deforming under plane-stress conditions, adapting a Coffin-Manson law as a failure criterion and using cumulative damage theory, a theoretical analysis has been developed for predicting the number of cycles for microcrack initiation in the presence of porosity. The predictions, which rely on pore shapes and the low cycle fatigue response of the fully dense matrix, accurately predict the number of cycles necessary to initiate a 15 micron crack adjacent to both isolated and interconnected pores during low cycle fatigue.

INTRODUCTION

The in-service performance of powder-processed as well as cast materials is frequently limited by the presence of processing defects such as porosity. Numerous investigations have examined the deleterious effects of porosity on high cycle fatigue and

---

[+] Currently: General Motors Technical Center, Warren, MI.

uniaxial tension behavior; for example see Refs. (1-15). The reductions in high cycle fatigue life of porous specimens have been attributed to local stress concentrations near pores which result in localized slip even though the nominal stress remains elastic. Although there have been many studies investigating the effects of porosity on high cycle fatigue behavior, there have been no fundamental studies which examine the effects of porosity on low cycle fatigue behavior. This is significant since the resistance of materials to low cycle fatigue failure, wherein the material is fully plastic, is often quite different than the response to high cycle fatigue when the nominal applied stress is elastic.

Previous studies of porosity on tensile fracture of porous materials suggest that low cycle fatigue may be sensitive to the presence of porosity; for example see Ref. 7. These studies have shown that during monotonic tension, pore-induced shear localization plays an important role in the linking of pores which results in a reduction in the tensile ductility. Thus, these results suggest that porosity could also be detrimental to low cycle fatigue life if strain localization develops near or between pores, as in tensile deformation. In fact, there are reports that porosity accelerates the failure process during low cycle fatigue[17-19] but these studies did not examine the problem in a systematic or fundamental manner.

The purpose of this investigation is to examine in detail the influence of rounded porosity on crack initiation during low cycle fatigue. Both experimental data and analytical predictions are presented. The effect of porosity on short crack growth at large strain amplitudes is reported elsewhere[20], and the overall influence of porosity on LCF will be described later.[21] The study utilizes powder-processed titanium containing well rounded pores with levels ranging from 0.4 to 6.0 volume percent. Isolated as well as continuous porosity conditions are examined. Although this study is based on titanium, the results should apply to other powder-processed or cast metals containing porosity so long as pore shapes and the cyclic flow characteristics of the matrix can be characterized and pore contents are sufficiently low, probably $\lesssim 10\%$, so that crack initiation occurs predominantly near individual pores.

EXPERIMENTAL PROCEDURE

Conventional powder metallurgy processing techniques using the sequential processes of cold isostatic pressing, sintering, swaging, and resintering were used to prepare low cycle fatigue specimens of commercially pure titanium, which was utilized as a model material for this study. The processing histories of the materials as a function of pores content are described elsewhere.[22] Wrought titanium having essentially the same impurity content as the powder-processed specimens was used for comparing the fatigue properties of the fully dense and porous conditions. In all cases, the materials contained between 0.13 and 0.15wt% oxygen.

The fully dense and porous microstructures containing 0.4%, 1.5% and 6% isolated porosity as well as 6% interconnected porosity are shown in Fig. 1. Stereopycnometer results confirmed that the pores were isolated in all but the "interconnected" condition, Fig. 1e. The microstructures in the isolated porosity specimens consist of well-rounded elliptical pores having average radius* of 10 to 15 microns and an average aspect ratio (major/minor diameter) of 1.3. Fig. 1e shows that when the interconnected-porosity specimens are examined in cross section, the pores have an average radius of about 25 microns and are somewhat less rounded than in the isolated case, having an average aspect ratio of 1.9. It should also be noted that the grain sizes were of the same order of magnitude in size as the pores in the fully dense and 6% isolated porous materials (40 μm grain size), but grain sizes of 140 μm were observed after processing the 0.4% porous condition.

Fully reversible low cycle fatigue tests were performed at room temperature in total strain control at strain ranges of .75 and 1.5%. The lower strain-range tests were

* The average radius is the average value of the Martin radii. In this study, the Martin radii are defined as the distance from the center of gravity of the pore to its edge; the initial radius measurement is taken at an arbitrary angle of 0° after which the remaining radii are obtained at angles of 45°, 90°, 135°, 180°, 225°, 270°, and 315°.

conducted at a frequency of .25 Hz while the larger amplitude tests have been performed at .15 Hz, both with a triangular waveform. Cylindrical push-pull low cycle fatigue specimens were used in this study; the specimens had a gage length of 15 mm and a 6.4 mm diameter. A lengthy (8-10 hr per specimen) polishing technique involving a combination of mechanical and chemical polishing was developed[22] to prepare the specimen surfaces for not only the fatigue testing but also for the surface replication analyses described below. Subsequent to this specimen preparation but prior to testing, the specimens were vacuum annealed at 700°C for 0.5 hr at a pressure of 3×10^{-3} Pa.

In order to monitor fatigue crack initiation, the low cycle fatigue tests were periodically interrupted and acetate surface replicas were taken. During each interruption the entire gage section of the specimen was examined using a replicating technique which was developed utilizing a surface replicating application tool. The tool consists of a cylindrical shell of brass with an inner layer of polymeric material (Tygon™) whose inner radius equals that of the gage section of the specimen. The combination of the flexible polymer and the rigid brass distributed loads to the replicating tape uniformly over a relatively large area while allowing the acetate tape to flow against the surface features. After application, the replicas were flattened and stored for analysis using a procedure described elsewhere.[22]

RESULTS AND DISCUSSION

a. Experimental Results

Porosity causes large reductions in low cycle fatigue (LCF) life at both of the strain amplitudes examined and for all of the porous conditions. Fig. 2 demonstrates that low cycle fatigue life deteriorates rapidly with increasing pore volume fraction, the effect being more pronounced when the porosity is interconnected and less well rounded. In order to analyze the fundamental causes for these large reductions in fatigue life, each of the failure stages of LCF must be examined. Low cycle fatigue failure may be separated into four

stages which typically overlap each other: (1) microcrack initiation, (2) microcrack (or short crack) growth, (3) microcrack linking, and (4) macrocrack propagation. Acceleration of any of these failure stages will result in a reduction of LCF life provided that no deceleration of any other stage occurs, which is usually unlikely.

Fig. 3 indicates the experimentally observed reduction in LCF life due to enhanced microcrack initiation when porosity is present. As shown in Fig. 3, the number of cycles to initiate a 15 μm microcrack decreases by roughly a factor of ten at both the 0.75 and 1.5% total strain ranges. The decrease in the number of cycles to initiate a crack is even greater, roughly a factor of 10^2, for the case of interconnected porosity when the pores have aspect ratios of roughly 1.9 compared to 1.3 in the isolated pore case. For the case of the isolated porous specimens, crack initiation appears essentially independent of pore level; see Fig. 3.

In all cases in this study, crack initiation occurs adjacent to pores, such as is shown in Fig. 4. Crack initiation occurs at or very near the specimen surface with most cracks initiating at individual pores at the porosity levels examined in this study ($\leq 6\%$). It is likely that at higher pore contents crack initiation between clusters of pores will become a dominant feature. The short cracks also tend to initiate on planes whose surface traces are normal to the stress axis. Dogleg cracks are quite common as the short cracks propagate across grain boundaries. It is interesting to note that despite observations of thousands of microcracks, seldom are cracks less than 15 μm in length observed.

b. Qualitative Analysis

The acceleration of the microcrack initiation process in this study is caused by pore-induced strain concentrations developing within a plastic matrix. Such a conclusion is consistent with the results of studies investigating (a) the influence of porosity[8-15] or (b) notches (or holes)[23-28] on high cycle fatigue behavior. Several studies[8-15] which have examined the influence of porosity on high cycle fatigue behavior have observed large decreases in fatigue life. The reductions in high cycle fatigue life were attributed to an

acceleration in the initiation of microcracks at pores due to the development local regions of pore-induced plasticity in a nominally elastic matrix. Furthermore, high cycle-fatigue studies of the influence of notches (or holes) have also shown that the microcrack initiation process is accelerated.[23-34] The acceleration in microcrack initiation once again is attributed to the development of local regions of plasticity in an elastic matrix as a result of stress concentrations which are generated at the stress riser (i.e. a notch or hole) during testing. Finally, it is significant that several investigations[25-30] have also shown that the high cycle fatigue life at the root of a notch (i.e. microcrack initiation) is approximately the same as for a fully dense material which is subjected to the same strain amplitude being generated near a stress riser.

All of the above analyses rely on the stress and strain concentrations which exist near pores, notches, or holes. Extension of that reasoning to the present study indicates that the large strain amplitudes developing adjacent to the pores cause local failure, i.e., the initiation of a crack. However, this study differs from those described above since the matrix, which contains the stress concentrators (i.e. pores), is subjected to fully plastic deformation. The following section presents an analysis of this form of crack initiation.

c. A Model for Pore-Induced Crack Initiation During LCF

In order to estimate the number of cycles necessary to initiate a 15μm long crack from a pore during fully plastic, low cycle fatigue, we consider three critical aspects:

(1) The first aspect of microcrack initiation is the characterization of local strains near pores at the specimen surface deforming in a plane stress condition. In the present analysis, we estimate the strain distributions adjacent to pores on the specimen surface by considering local strains near through-thickness elliptical holes in a fully plastic sheet deforming under plane stress conditions. In this case, the theoretical stress/strain concentration analysis proposed by Neuber[35] may be used to predict the local plastic strain amplitude profiles near a hole provided that the hole geometry and the matrix stress-strain responses are known. Assuming the strains near a pore intersecting a free surface

are similar to those of a hole in plane stress, we can utilize the predicted strain profiles to estimate the strain distributions adjacent to an isolated pore located on the surface. Since the local strain amplitudes near the holes (pores) can be determined as a function of cycles and distance from the pore, they can be incorporated into a plastic strain-life analysis to predict local failure (crack initiation).

(2) In the next aspect, the theoretically predicted plastic strain amplitudes during each cycle are used to estimate the number of cycles to failure for the material in the region adjacent to the pore. The failure estimates are based on the maximum local strain amplitude which develops at the pore surface on the plane of maximum strain concentration. The microcrack initiation predictions are based on a local failure criterion utilizing the Manson-Coffin relationship[36,37] for fully dense titanium.[38]

(3) The final aspect uses a cumulative damage theory to estimate the number of cycles to initiate a crack by incorporating the low cycle fatigue failure predictions of the material adjacent to the pore after each cycle. This is necessary because the imposed, macroscopic plastic strain amplitude varies during cycling due to cyclic hardening followed by cyclic softening[39].

The first aspect of the microcrack initiation model relies on a prediction of the local plastic strain amplitude profiles adjacent to a pore at the specimen surface. As discussed in (1) above, we may estimate those strain profiles by utilizing a solution for the plastic strain distributions near a through-thickness hole in the same material deforming under plane stress conditions. This is done through the use of Neuber's analysis[35] in which the stress concentration K_{cl} at a hole:

$$K_{c1} = \sqrt{K_\sigma K_\varepsilon} \qquad (1)$$

where $K_\sigma = \sigma_l/\sigma_{nom}$ = local stress/nominal stress at infinity, and

$K_\varepsilon = \varepsilon_l/\varepsilon_{nom}$ = local strain/nominal strain at infinity

In Eq. 1, K_{el} is the stress concentration adjacent to the defect, which is a function of position, and K_σ and K_ε are the local stress and strain concentrations developed near a defect for any deformation state, including plastic deformation. In order to solve Eq. 1 in a plastically deforming matrix it is necessary to relate the stress and strain in the region near the defect assuming the material obeys a stress σ-strain ε relationship such as:

$$\sigma = C\varepsilon^n \tag{2}$$

In Eq. 2, C and n are the empirically fitted strength coefficient and work-hardening exponent, respectively. Upon substituting the results into Eq. 1 and solving for the plastic local strain, we obtain

$$\varepsilon_l = (K_{e_l}^2 * \{\Delta\varepsilon_{NOM}\}^{(n+1)})^{(\frac{1}{n+1})} \tag{3}$$

In Eq. 3, ε_l is the local strain adjacent to the defect, and $\Delta\varepsilon_{NOM}$ is the nominally applied strain. Further work by Seeger and Heuler[34] indicated that in order to improve the results from the Neuber analysis, the reduction in cross-sectional area must also be accounted for in a specimen of finite width. In the present case of pores which are infinitesmal in size and uniform in spatial distribution, the correction for specimen width is not necessary.

The solution to Eq. 3 for the local strain distribution adjacent to a defect is complex in the present case because of the form of K_{el} for a through-thickness elliptical hole in a uniformly stressed plate. In this case, K_{el} is obtained from elasticity theory and is given by[40]

$$K_{el} = \frac{\sinh(2\alpha) + \cos(2\beta) - e^{(2\alpha)} \cos 2(\beta - \eta)}{\cosh(2\alpha) - \cos(2\eta)} \tag{4}$$

where α and ν describe the stress field as a family of intersecting ellipse and hyperbolas by the use of curvilinear coordinates, and β is the angle (in radians) between the applied stress and the major axis. A rigorous derivation of the stress distributions generated adjacent to an elliptical-through-thickness hole during monotonic deformation is described in Ref. 40. The combination of Eq. (3) and (4) provides solutions which predict pseudo-plasticity strain distributions not only for different elliptical shapes but may also be used to predict the effects of changes in shape during deformation. In addition, this analysis will predict the strain profile on any plane in the region.

Before Eq. 3 is applied to the LCF analysis, it is instructive to verify its predictive capabilities for plastic strain distributions near holes not only during monotonic straining but also after cyclic strain of a LCF specimen. It should be noted that several previous investigators have applied the Neuber analysis (with varying degrees of success) to predict stress and strain concentrations at notches in low and high cycle fatigue.[41] In the case of monotonic tension, a comparison of the theoretical and experimental plastic strain distributions near a through-thickness hole (initially circular) in sheet specimens of 70-30 brass, 1100 Al, and a low carbon steel will be reported elsewhere.[42] Agreement between the predicted and observed is good for all three materials, especially at small macroscopic nominal strains, such as $\varepsilon_{nom} = .03$.

For cyclic straining, Fig. 4 shows a comparison of predicted and observed strain distributions near a circular hole in titanium specimens subjected to 1.5% total strain amplitude. In this instance, the cyclic strain-hardening exponent ($n = .275$[43]) is used in Eq. 2 and the nominal strain in Eq. 3 is the plastic strain amplitude. Fig. 4 indicates a reasonably good level of agreement between predicted and observed strain distributions, despite scatter in the experimental data. Since a crack was detected at 60 cycles, the strain distribution data indicate no significant strain accumulation occurred near the hole until about 80% of the local fatigue life (i.e., 50 cycles). This result is in agreement of Quesnel

and Meshi[41] who also observed an accumulation in local strain just prior to crack nucleation during high cycle fatigue testing in the presence of a hole. Thus, we conclude that Eq's. 3 and 4 provide reasonable estimates of the local strain amplitudes adjacent to holes in strain-hardening materials undergoing LCF for most of the life of the material.

To incorporate the Neuber analysis into a model which predicts crack initiation during LCF, we assume a strain-based failure criterion for local fracture (i.e., microcrack initiation) adjacent to a hole/pore. In the present case, that criterion relies on Manson-Coffin relationship[36,37] for fully dense titanium:

$$(\Delta\varepsilon p/2)(N_f) = C^b \tag{5}$$

where $\Delta\varepsilon p/2$ is the plastic strain amplitude, N_F is the number of cycles to failure, and C and b are material constants which have been determined for the fully dense titanium. As determined in the present study, the values of C and b at the onset of macrocrack propagation are 23% and -0.51, respectively; these are in good agreement with another investigation[38]. To improve the applicability of Eq. 5 to the present analysis, the constants have been determined at the onset of macrocrack propagation and do not include the number of cycles for macrocrack crack propagation. In addition, the plastic strain amplitude $\Delta\varepsilon p$ has to be evaluated as a function of cycles due to cyclic hardening or softening. Thus, in these total strain amplitude tests, the plastic strain amplitude must be evaluated as a function of cycles in order that the equation can be correctly implemented. It should be recognized that implicit in the use of Eq. 5 is the assumption that the life of the material at the base of a strain concentrator, such as a pore, will be the same as that of a smooth LCF specimen.

In order to imitate the fatigue life of a strip of material adjacent to a pore, a cumulative damage model must be implemented because of the variability of strain amplitudes during cycling. A cumulative damage theory must thus be used to estimate the fatigue life of the

material near the pore (i.e. microcrack initiation) which has deformed under locally varying strain amplitudes* . In the present study, the pertinent relationship is

$$(N_1/N_{F1}+N_2/N_{F2}+...+N_x/N_{Fx}) = 1.0 \quad (6)$$

In Eq. 6, N_x is the number of cycles a specimen is cycled at a particular strain amplitude $\Delta\varepsilon_x$, while N_{Fx} is the number of cycles to failure as predicted by the Manson-Coffin equation for a specimen cycled to failure at a strain amplitude $\Delta\varepsilon_x$.

In order to utilize Eq's. 2-6, we assume that the strain distribution near a microscopic pore intersecting a free surface are similar to those adjacent to an elliptical hole in a metal deforming under plane stress conditions. Furthermore, since cracks tend to initiate adjacent to pores along a plane bisecting the pore and normal to the stress axis, the strain distributions along the corresponding plane near a hole, such as in Fig. 5, are used in the analysis. The analysis ignores scaling effects such as the differences in plasticity when the pore size is roughly that of the grain size and local plasticity effects when only a few grains are involved. The analogy between a through-thickness hole and a pore intersecting a surface may be better than it seems at first glance. In the case of continuous porosity, the geometries clearly approximate each other; even in the discontinuous pore case, most of the pores at which cracks initiate are relatively deep compared to their diameter, thus approximating a hole intersecting the surface.

Given the above assumptions, an estimate can be made of the number of cycles to initiate a crack adjacent to a pore. Specifically, this requires the use of Eqs. 2-6, the cyclic stress-strain response of fully dense Ti as given by Eq. 5, and approximating the pores as elliptical holes. It should be recalled that the pore shapes are elliptical in cross section with the ratio of the major to minor diameters being 1.3 and 1.9 for the isolated and

* The variation in local plastic strain amplitude at any selected distance from the pore can be a result of the titanium cyclically hardening or softening during the lows cycle fatigue tests. Whether cyclic hardening, and or, softening occurs depends on the strain amplitudes at which the tests are performed.[39]

interconnected porous materials, respectively. We also assume that the crack will initiate at a pore surface at the maximum strain amplitude location (note: as before, this occurs on a plane normal to the fatigue axis which bisects the pore). Thus, in order to estimate the number of cycles to initiate a microcrack, the maximum plastic strain obtained at the surface of a specially oriented pore (i.e. major axis perpendicular to the fatigue axis) has been chosen.

The theoretical estimates of the number of cycles to initiate an infinitesimally small microcrack at the surface of a pore are presented in Fig. 3 along with the previously described experimental data for cracks 15 microns in length. The theoretical and experimental results presented in Fig. 3 are in excellent agreement for the materials containing isolated- and interconnected-porosity at both strain amplitudes. It should be emphasized that no adjustable parameters are used to force a fit in the analysis. Only the Manson-Coffin parameters, the cyclic stress-strain response, and cyclic strain amplitudes (which are used in the cumulative damage aspect), and the pore geometries used in calculating the local strain distributions need to be specified.

The choice of a 15 micron crack as the critical size for the microcrack initiation is based on the fact that very few cracks below this size were detected among several thousand cracks examined. The absence of cracks below 15 microns in size is probably due to the steep local strain gradient present in the pore-induced plastic zone. Data such as that in Fig. 5 strongly suggest that the steep gradients in the pore-induced local plastic zones extend at least one pore radius into the material. Given a typical pore diameter of 30 μm, tnis implies a strip of material of 15 to 20 μm from the pore surface within which the large local plastic strain amplitudes cause large accelerations in the microcrack growth, as has been noted elsewhere in the presence of notches.[24-28]

CONCLUSIONS

The influence of porosity on crack initiation during low cycle fatigue has been studied using powder-processed titanium containing rounded porosity ranging from 0 to 6% by volume as a model system. Experimental results from low cycle fatigue testing at total strain ranges of 0.75 and 1.5% at 25°C indicate the following.

(a) The enhancement of crack initiation due to porosity results in significant reductions in low cycle fatigue life. For all the levels of porosity examined, the number of cycles necessary to initiate at 15 micron crack decreased by roughly an order of magnitude or more.

(b) The acceleration of microcrack initiation is a result of pore-induced plastic zones which create locally high regions of plastic strain at or very near the specimen surface adjacent to the pore. An analysis suggests that the localized plasticity extends into the matrix material roughly two to three pore radii beyond the edge of a pore on the plane of maximum strain concentration.

(c) For the isolated-porous materials in which the porosity maintains similar geometries, the enhancement of microcrack initiation is essentially independent of the porosity levels at the strain amplitude examined.

(d) When the porosity is interconnected and the pores tend to be more elongated, the microcrack initiation process is further enhanced probably as a result of the pores having a higher aspect ratio than those in the isolated porous materials.

An analysis of pore-induced microcrack initiation has been successfully performed on the following basis:

(a) The local strain distributions near pores on the free surface of a plastically deforming matrix have been modeled utilizing a through-thickness elliptical hole in a deforming matrix material under plane stress conditions. Good agreement between experimentally measured and theoretically determined (using a Neuber analysis[35]) strain profiles adjacent to elliptical holes has been obtained for matrices subjected to uniaxial

tension as well as low cycle fatigue deformation. The theoretical analysis relies only on the knowledge of the cyclic stress-strain response of the matrix and the hole shape. A significant experimental observation is that very little strain accumulation occurs adjacent to a hole during LCF until approximately 80% of the life of the strip of material local to the hole.

(a) Using a Manson-Coffin relationship as a criterion for local failure (crack initiation) in conjunction with a cumulative damage law, the number of cycles to initiate a 15 μm crack can be predicted from estimates of the maximum strain amplitudes near pores, with elliptical cross sections intersecting the free surface. Assuming no scaling effects and that strain distributions at free surfaces near microscopic pores are similar to those near macroscopic through-thickness holes, we obtain very good agreement between predictions and experimental observations of the number of cycles to initiate a 15 μm crack in the presence of porosity during LCF.

REFERENCES

1. H. A. Kuhn and C. L. Downey, Int. J. of Powder Metal. 7(1), 15-25 (1971).
2. G. A. Doshchinskii, V. Z. Midukov, V. S. Golovenko and P. A. Kornienko, Translation of Problemy Prochnosti, 12, pp. 36-39 (1974).
3. H. E. Exner and D. Pohl, Powder Metal. Int., 10(4), 193-196 (1979).
4. R. Haynes, Powder Metal., 1, pp. 17-20 (1977).
5. M. Eudier, Powder Metal., 9, pp. 278-290 (1962).
6. B. Karlsson and I. Bertilsson, Scandinavian J. of Metall., 11 (6), pp. 267-275 (1982).
7. R. J. Bourcier, D. A. Koss, R. E. Smelser and O. Richmond, Acta Metall. 34(12), pp. 2443-2453 (1986).
8. F. Soniak and L. Remy, The Behavior of Short Fatigue Cracks, EFG Pub. 1, Eds. K. J. Miller and E. R. de los Rios, Mechanical Engineering Publications, London, pp. 115-132 (1986).

9. A. Fathulla, B. Weiss and R. Stickler, The Behavior of Short Fatigue Cracks, EFP Pub. 1, Eds. K. J. Miller and E. R. de los Rios, Mechanical Engineering Publications, London, pp. 115-132 (1986).

10. D. Eylon, Y Mahajan, N. R. Ontko and F. H. Froes, Proc. AIME Symp. on Titanium Powder Metallurgy (1980).

11. P. R. Smith, D. Eylon, S. W. Schwenker and F. H. Froes, Advanced Processing Methods for Titanium, Eds. D. F. Hasson and C. H. Hamilton, From TMS of AIME held in Louisville, KY, October 191, pp. 61-77.

12. N. A. Fleck and R. A. Smith, Powder Metal., 3, pp. 121-125 (1981).

13. N. A. Fleck and R. A. Smith, Powder Metal., 24(3), pp. 126-130 (1981)

14. R. S. Bankowski and W. H. Feilbach, Int. J. of Powder Metall., 6 (3), pp. 23-37 (1970).

15. P. DiMascio and R. A. Queeney, Int. J. of Powder Metall. & Powder Tech., 19(2), pp. 127-135 (1983).

16. S. Bash, P. Taupin and S. D. Antolovich, Metall. Trans A, 10A, pp. 1481-1490 (1979).

17. J. M. Hyzak and I. M. Bernstein, Metall. Trans. A, 13A, pp. 33-43 (1982).

18. J. M. Hyzak and I. M. Bernstein, Metal. Trans. A, 13A, pp. 45-52 (1982).

19. K. Majima, A. Tokuda, and K. Shoji, Japan Soc. of Powder and Powder Metall. 32, 158-163 (1985) and 164-168 (1985).

20. D. A. Gerard and D. A. Koss, Technical Report No. 10, Office of Naval Research Contract No. NOOO14-86-K-0381, July 1988.

21. D. A. Gerard and D. A. Koss, unpublished research, 1989.

22. D. A. Gerard, Ph.D. Thesis, Michigan Technological University, 1989.

23. O. Oni and C. Bathias, The Behaviour of Short Fatigue Cracks, European Group Fracture Pub. 1, Eds. K. J. Miller, and E. R. de los Rios, Mechanical Engineering Publications Limited, London pp. 295-307 (1986).

24. J. Foth, R. Marissen, K. H. Trautmann, and H. Nowack, ibid, pp. 3533-368.

25. P. Laor, H. Sehitoglu, and R. C. McClung, ibid, pp. 369-386.

26. H. Sehitoglu, Fracture Mechanics: Sixteenth Symposium, ASTM STP 868, M. F. Kanninen and A. T. Hopper, Eds, American society for Testing Materials, Philadelphia, PA, pp. 361-380 (1985).

27. F. Heubaum and M. E. Fine, Scripta Met., 18, pp. 1235-1240 (1984).

28. El Haddad, M. H. Smith, and T. H. Topper, Fracture Mechanics, ASTM STP 677, C. W. Smith, Ed., American Society for Testing Materials, Philadelphia, PA, pp. 274-289 (1979).

29. Y-S. Wu, Low Cycle Fatigue , ASTM STP 942, H. D. Solomon, G. R. Halford, L. R. Kaisand, and B. N. Leis, Eds., Am. Soc. for Testing and Materials, Philadelphia, pp. 1007-1021 (1988).

30. B. N. Leis, C. V. B. Gowda and T. H. Topper, from Cyclic Stress-Strain Behavior - Analysis, Experimentation, and Failure Prediction, ASTM, STP 519, L. F. Coffin and Erhard Krempl - symposium chairmen, pp. 1323-150 (1972).

31. J. H. Crews, Jr., Achievement of High Fatigue Resistance in Metals and Alloys, ASTM STP 467, Am. Soc. for Testing and Materials, pp. 37-52 (1970).

32. R. M. Wetzel, J. of Materials, JMLSA, 3 (3), pp. 646-657 (1968).

33. J-D. Morrow, R. M. Wetzel and T. H. Topper, Effects of Environment and Complex Load History on Fatigue Life, ASTM STP 462, Am. Soc. for Testing and Materials, pp. 74-91 (1970).

34. T. Seeger and P. Heuler, J. of Testing and Evaluation, JTEVA, 8 (4), pp. 199-204 (1980).

35. H. Neuber, Transactions of the ASME, pp. 544-550 (1961).

36. J. F. Tovernelli and L. F. Coffin, Jr., Jour. of Basic Eng., Trans AIME 84, 533 (1962).

37. S. S. Manson, Experimental Mech. 5, 193 (1965).

38. M. J. Douglas and A. Plumtree, Fracture Mechanics, ASTM STP 677, C. W. Smith, Ed., American Society for Testing Materials, Philadelphia, PA, pp. 68-84 (1979).

39. J. I. Dickson, J. Ducher, and A. Plumtree, Metall. Trans A 7A, 1559 (1976).

40. S. P. Timoshenko and J. N. Goodier, Theory of Elasticity, McGraw Hill, New York, 1970, pps. 187-196.

41. D. J. Quesnel and M. Meshii, Jour. of Testing and Evaluation, 4, 319-326 (1976).

42. D. A. Gerard, P. E. Magnusen, and D. A. Koss, unpublished research.

43. A. Puskar, Materials Sci. and Eng. 61, pp. 111-116 (1983).

List of Figures

Figure 1 Polarized light micrographs of titanium containing (a) 0% porosity, (b) 0.4% isolated porosity, (c) 1.5% isolated porosity, (d) 6% isolated porosity, and (e) 6% interconnected porosity. The bright reflections are from the epoxy used to preserve the original pore shape during polishing. All the micrographs have the same magnification.

Figure 2. The influence of porosity on low cycle fatigue life for titanium subjected to total strain range testing at (a) 0.75%, and (b) 1.5%.

Figure 3. A comparison of the experimental results and theoretical predictions for the number of cycles to initiate a 15 μm crack in the fully dense and porous materials during total strain range testing at (a) 0.75% and (b) 1.5%.

Figure 4. Micrographs of surface replicas showing microcracks which have initiated adjacent to pores during low cycle fatigue.

Figure 5. A comparison of the theoretical and experimental total strtain profiles adjacent to a circular hole on the plane bisecting to hole and normal to the stress axis at the maximum tensile reversal after selected cycles for a 1.5% total strain range test. The hole-to-specimen-width ratio was twenty percent and R/R(o) refers to the ratio of the distance R from the hole center as normally to hole radius R(o).

List of Figures

Figure 1 Polarized light micrographs of titanium containing (a) 0% porosity, (b) 0.4% isolated porosity, (c) 1.5% isolated porosity, (d) 6% isolated porosity, and (e) 6% interconnected porosity. The bright reflections are from the epoxy used to preserve the original pore shape during polishing. All the micrographs have the same magnification.

Figure 2. The influence of porosity on low cycle fatigue life for titanium subjected to total strain range testing at (a) 0.75%, and (b) 1.5%.

Figure 3. A comparison of the experimental results and theoretical predictions for the number of cycles to initiate a 15 μm crack in the fully dense and porous materials during total strain range testing at (a) 0.75% and (b) 1.5%.

Figure 4. Micrographs of surface replicas showing microcracks which have initiated adjacent to pores during low cycle fatigue.

Figure 5. A comparison of the theoretical and experimental total strtain profiles adjacent to a circular hole on the plane bisecting to hole and normal to the stress axis at the maximum tensile reversal after selected cycles for a 1.5% total strain range test. The hole-to-specimen-width ratio was twenty percent and R/R(o) refers to the ratio of the distance R from the hole center as normally to hole radius R(o).

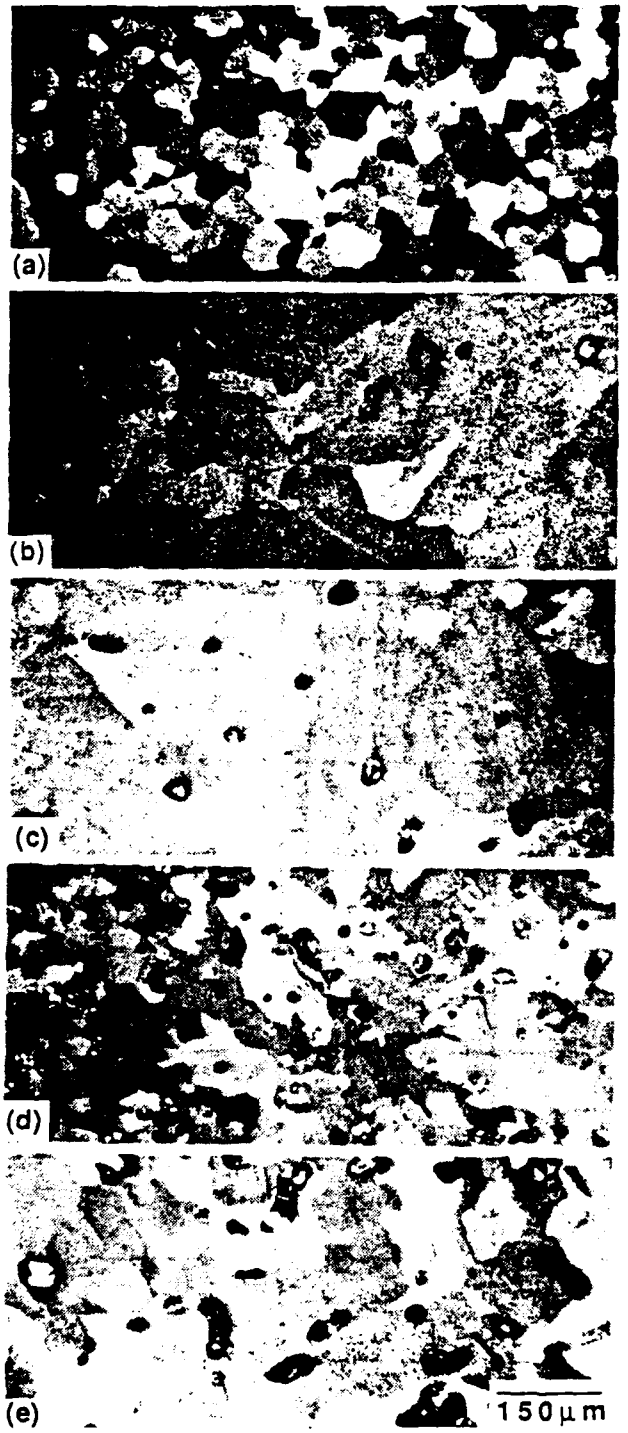

Figure 1 Polarized light micrographs of titanium containing (a) 0% porosity, (b) 0.4% isolated porosity, (c) 1.5% isolated porosity, (d) 6% isolated porosity, and (e) 6% interconnected porosity. The bright reflections are from the epoxy used to preserve the original pore shape during polishing. All the micrographs have the same magnification.

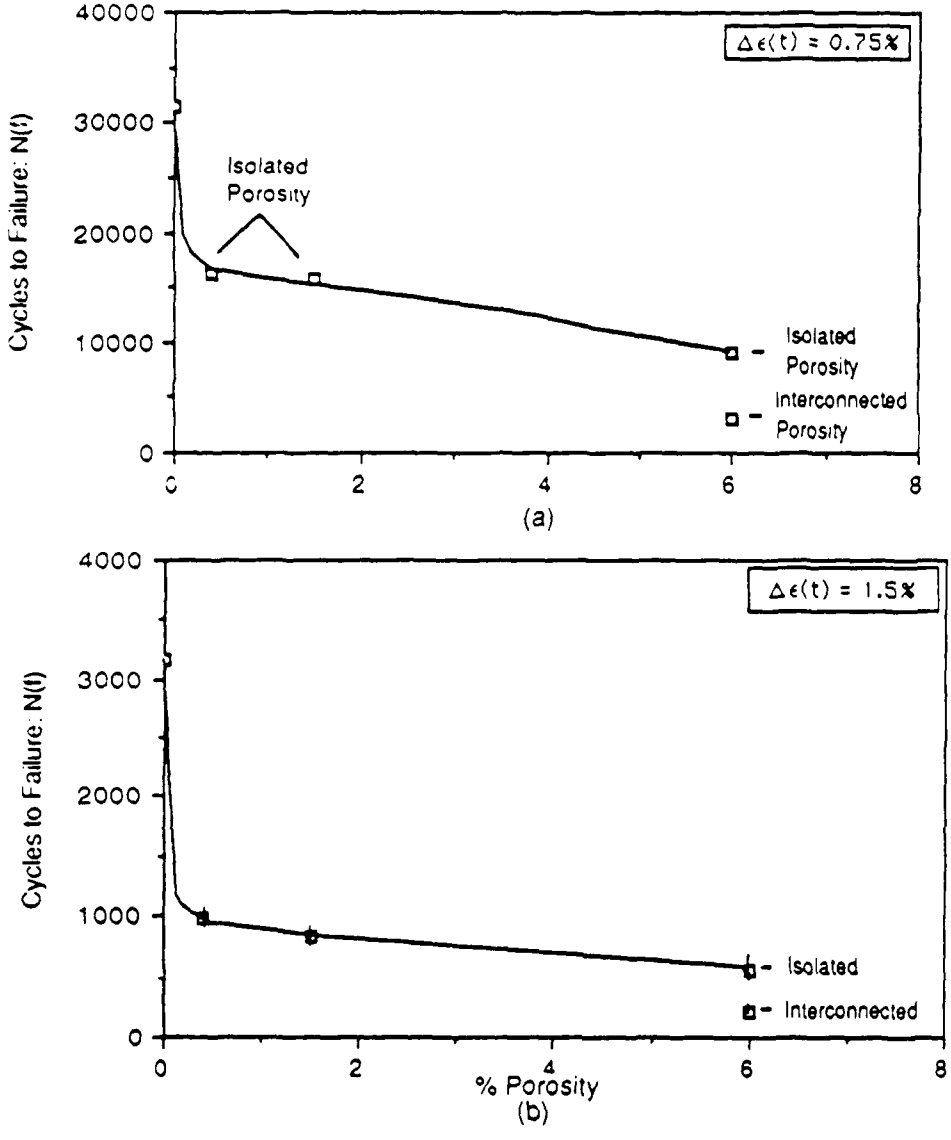

Figure 2. The influence of porosity on low cycle fatigue life for titanium subjected to total strain range testing at (a) 0.75%, and (b) 1.5%.

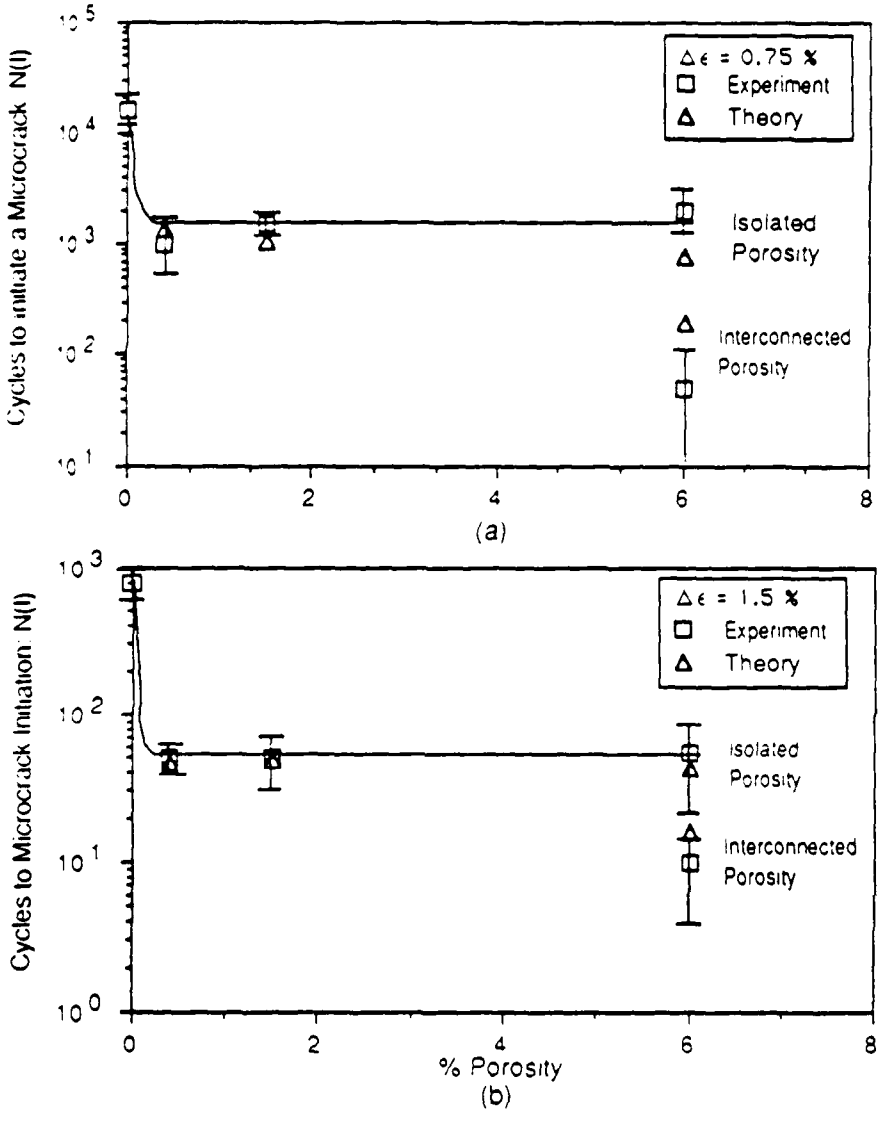

Figure 3. A comparison of the experimental results and theoretical predictions for the number of cycles to initiate a 15 μm crack in the fully dense and porous materials during total strain range testing at (a) 0.75% and (b) 1.5%.

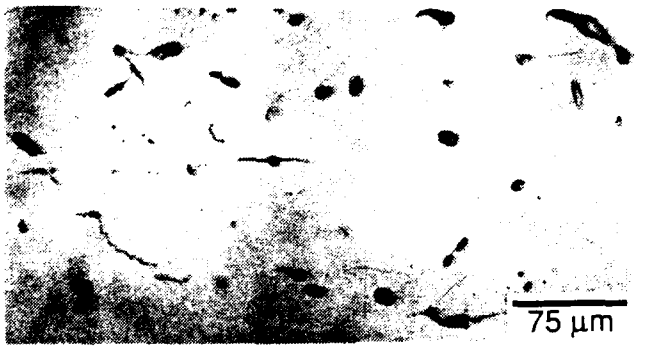

Figure 4 Micrograph of a surface replica showing microcracks initiated at pores in the 6% porous titanium (isolated porosity). The stress axis is vertical.

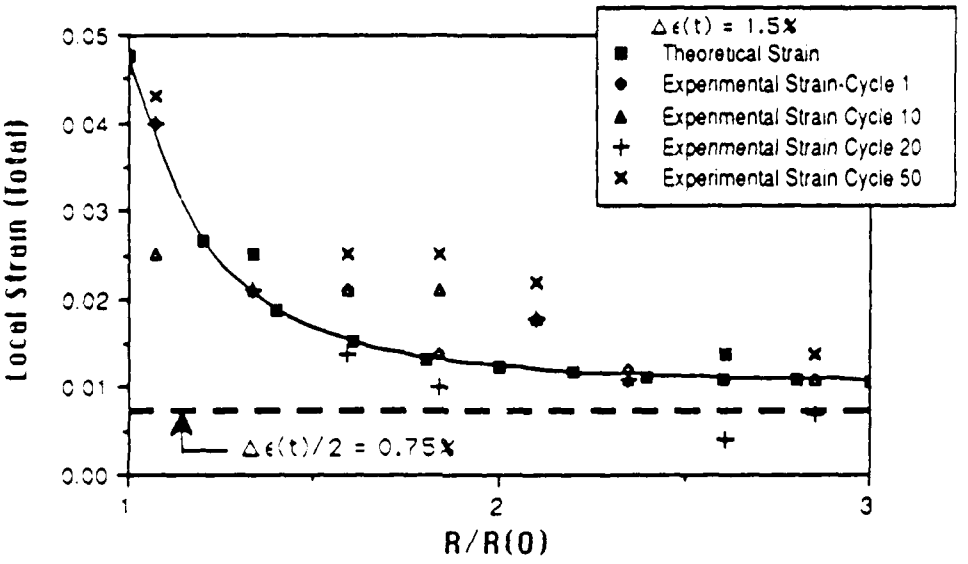

Figure 5. A comparison of the theoretical and experimental total strain profiles adjacent to a circular hole on the plane bisecting to hole and normal to the stress axis at the maximum tensile reversal after selected cycles for a 1.5% total strain range test. The hole-to-specimen-width ratio was twenty percent and R/R(o) refers to the ratio of the distance R from the hole center as normally to hole radius R(o).